arXiv:1605.06771v1 [quant-ph] 22 May 2016

Simple source for large linear cluster photonic states

Y. Pilnyak, N. Aharon, D. Istrati, E. Megidish, A. Retzker, and H. S. Eisenberg

Racah Institute of Physics, Hebrew University of Jerusalem, Jerusalem 91904, Israel

The experimental realization of many-body entangled states is one of the main goals of quantum technology as these states are a key resource for quantum computation and quantum sensing. However, increasing the number of photons in an entangled state has been proved to be a painstakingly hard task. This is a result of the non-deterministic emission of current photon sources and the distinguishability between photons from different sources. Moreover, the generation rate and the complexity of the optical setups hinder scalability. Here we present a new scheme that is compact, requires a very modest amount of components, and avoids the distinguishability issues by using only one single-photon source. States of any number of photons are generated with the same configuration, with no need for increasing the optical setup. The basic operation of this scheme is experimentally demonstrated and its sensitivity to imperfections is considered.

The majority of quantum information protocols require entanglement between different subsystems of a quantum state[1]. For example, the demonstration of a useful quantum computer, will involve the controlled entanglement of probably thousands of quantum elements[2]. This has been proved so far to be a very hard task, especially with photons whose generation rates decrease exponentially with their numbers[3]. This task is simplified when several single photon sources are combined on an optical chip through integrated waveguides[4], but the required complete indistinguishability between all of the sources is hard to achieve[5–10]. The highest numbers of entangled photons were created by combining polarization entangled photon pairs from several parametric down-conversion (PDC) sources[3]. Nevertheless, in order to increase the number of entangled photons, more sources, entangling operations, and matching delay lines are required. In addition, extremely low state detection rates were observed, due to the probabilistic nature of PDC, where typical photon-pair generation probabilities are of few percents. Previously, we demonstrated an approach that simplified this setup, such that only a single entangled photon pair source and a single delay line are required, regardless of the size of the generated state[11]. This setup still suffers from low generation rates, as it also uses PDC.

In this work we present a new scheme that generates multi-photon linear cluster states[12]. The scheme is using single photon sources[13], where on-demand operation is almost achieved[14–17], and a single delay line in a loop arrangement. Thus,the amount of resources is reduced to only one single-photon emitter and one entangling gate. Such delay loops were previously used in schemes where quantum information is time-bin encoded[18, 19]. The use of only a single source simplifies the efforts for indistinguishability, removing the need for fine and stable spectral tuning of the different sources[10, 20–22]. Nevertheless, consequent emissions still require indistinguishability. The typically long coherence times of such sources compared to PDC sources, imply even lower sensitivity to the length of the delay line. Furthermore, these sources' narrow spectral widths enable the use of optical fibers, which can not be used in the case of PDC photons due to dispersion induced distinguishability. This scheme requires a photon-photon entangling operation. Although there are many efforts to demonstrate a device with such interaction, there is still no practically satisfying demonstration[23–27]. Currently, the most efficient way to entangle the polarization of two photons is by post-selection of the state after passing through a polarizing beam-splitter (PBS)[28]. The post-selection step introduces a 50% success probability, but relatively high fidelities. Yet, whichever is the entangling process that is used, our scheme only requires such a single device.

The main principles of our scheme are presented in Fig. 1. A single photon source emits a polarized photon into position 1. The photon reaches a CNOT entangling gate, but passes it through with no effect into the delay loop at position 2. Inside the loop, the photon is rotated by 45° with a half-wave plate and arrives to position 3. Synchronized with the second arrival of this photon to the entangling gate, the single photon source is triggered again such that the two photons are simultaneously entering both input ports of the entangling gate at positions 1 (target) and 3 (control). The CNOT gate generates entanglement between the photon that has left the loop and the other one that is still inside it. After the photon inside the loop is rotated by the wave plate, the source is synchronously triggered for the third time. This time, the entangling operation combines the new photon with the previous state and creates a three photon GHZ state[29] Continuing this process successively, results in an ever growing chain of entangled photons in a linear cluster state. The delay loop serves as a quantum memory that connects between generations, in a similar way to the entangled single-photon quantum dot source of the proposal in Ref. 30.

The output stream of photons is analyzed at different polarization bases by rotating the photon polariza-

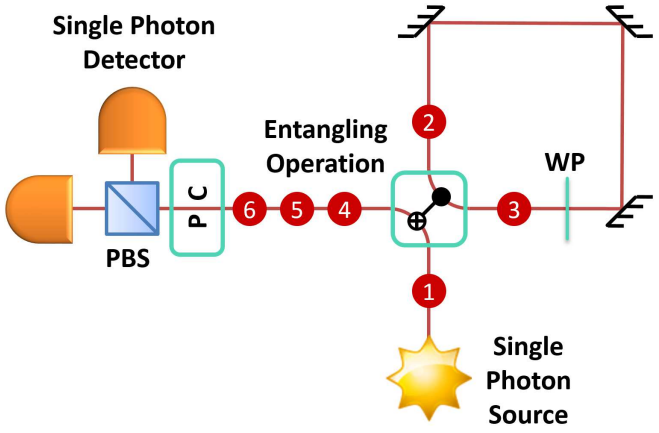

FIG. 1. **A scheme for generating multi-photon cluster states.** A single-photon source emits photons consecutively into an optical path, leading into a Sagnac-like loop. Inside the loop there is a half-wave plate (WP) at 22.5°, and its delay time is matched to the time between consecutive photon emissions. At the point of intersection of the optical paths, a photon entangling operation entangles one photon from the source and another from the delay line. One photon continues into the delay loop and the other one further towards a polarization controller (PC), a polarizing beam splitter (PBS), and detectors. The state is characterized by different detection sequences. See main text for more details.

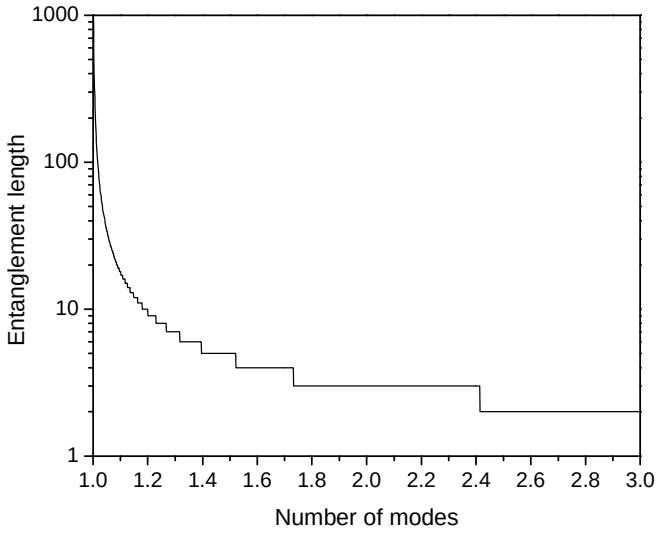

FIG. 2. **The entanglement length dependence on the number of modes.** The length of the longest generated chain where entanglement can be measured between its two end points. The minimal length 2 is attained for more than ~ 2.41 modes. For chains of at least 10, 84, and 825 photons, no more than 1.2, 1.02, and 1.002 modes are allowed, respectively.

tions with a polarization controller and detecting the photons at the output ports of a PBS. By using fast Pockels cells, it is possible to change the projection direction of some photons according to the previous measurement outcomes of others. This procedure is called 'feed forward', and it is required for quantum computation protocols using graph states[31].

We have considered several possible causes for state imperfections that can affect the presented scheme, such as photon partial polarization degree, probability to emit two photons simultaneously, imperfection of the entangling gate, and distinguishability between the photons[13]. The number of modes that a photon occupies $N_m = \frac{1}{1-g_0^{(2)}}$ can quantify distinguishability. The '*entanglement length*' was used to quantify the effects of various imperfections. This measure is defined as the length of the longest linear cluster, where the first and last photons have positive concurrence after all others were measured at the $\{|p\rangle = \frac{1}{\sqrt{2}}(|h\rangle + |v\rangle), |m\rangle = \frac{1}{\sqrt{2}}(|h\rangle - |v\rangle)\}$ basis, where $|h\rangle$ ($|v\rangle$) represent horizontal (vertical) polarization. Its dependence on the number of modes is presented in Fig. 2[32].

Currently, adequate on-demand single-photon sources are unavailable. Thus, we demonstrate our scheme using a heralded periodic PDC source. The heralded source generates two photons probabilistically. One photon is immediately detected, announcing the presence of its brother, which is the photon being used in the experiment (Fig. 3). Although this source is missing determinism - a key advantage of the proposed scheme, it is still instructive to demonstrate the basic operation of the scheme and some of its challenges.

The entangling operation in this demonstration is by post-selecting a single photon exiting each output port of a PBS[28]. This non-unitary operation entangles photons not as the desired CNOT gate. Nevertheless, as the source photon polarization is known, this difference has no consequences. The post-selection condition is fulfilled by requiring a sequential detection of photons. Whenever two photons leave the PBS from the same output port, there is a missing detection event. The PDC source can simultaneously emit two pairs, or an extra pair before or after the required sequence. Nevertheless, these are rare higher order events with almost no effect.

By scanning the delay loop length (Fig. 3), distinguishability between the two photons is controlled. Maximal indistinguishability, and thus, nonlocal interference, is achieved when the delay time matches the repetition rate of the pump laser. At this length, the photons that have already left the delay loop towards the detectors are entangled with the last photon which is still inside the loop. In order to detect entanglement, all photons should be observed at the $\{|p\rangle, |m\rangle\}$ basis by a half-wave plate rotation. The last photon which is still in the loop is observed by the first projecting PBS and the preceding wave plate. If this photon is detected within the consequent time slot, it was projected onto the $|p\rangle$ state, but otherwise, its projection was onto $|m\rangle$.

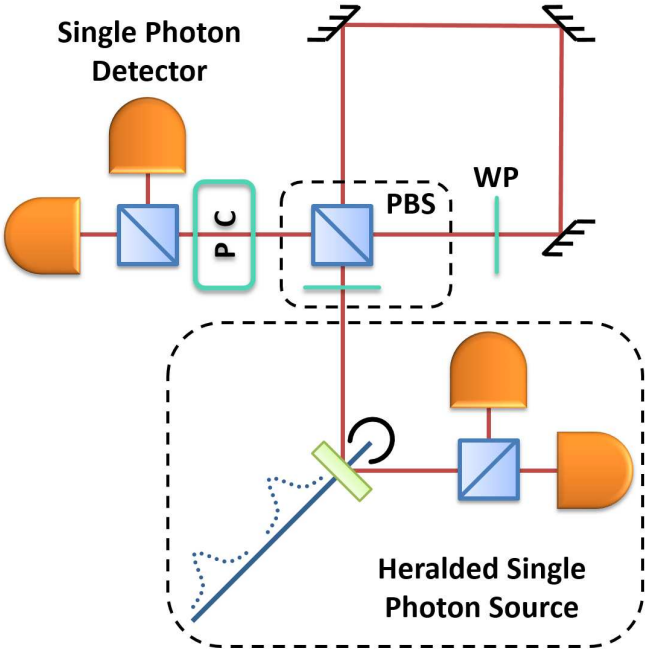

FIG. 3. **The optical setup used for demonstration of the scheme.** A heralded single-photon source is used, and the entangling operation is performed with linear optics and post-selection. A nonlinear BaB_2O_4 is pumped by a 390 nm double Ti:Sapphire laser.

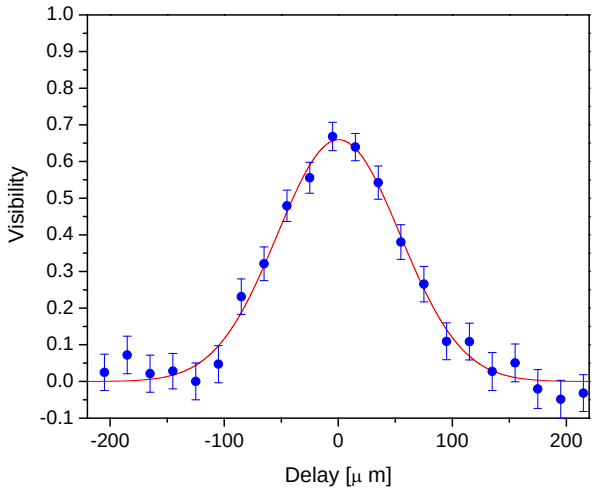

FIG. 4. **Nonlocal interference visibility between two entangled photons.** A constructive (destructive) interference is observed as the delay is scanned, for the $|\phi^+\rangle$ ($|\phi^-\rangle$) state. The fourfold signal is composed of the detection of the two heralding photons and the two entangled photons. Each data point was integrated over 16 minutes. Event rate was of 1 Hz at an average pump power of 350 mW. Errors are calculated assuming Poisson distribution.

The interference graphs of two and three photon states are presented in Figs. 4 and 5, respectively. When distinguishability is removed, some polarization sequences interfere constructively and some destructively. The two photon state interference visibility is $V_2 = 66 \pm 2\%$ and the three photon state visibility is $V_3 = 45 \pm 11\%$. We estimate that higher order events account for 5-10% of the two photon visibility degradation, as well as imperfect PBS performance. Nevertheless, spectral distinguishability is probably the major cause. Thus, it is possible to use V_2 to estimate the number of distinguishable modes to be $N_m = \frac{1}{V_2} \sim 1.5$, corresponding to an expected three photon visibility of $V_3 = V_2^2 = 44\%$, and maximum possible entanglement length of 5.

It is instructive to examine the prospects of currently available sources. Recently, high levels of indistinguishability have been demonstrated[17, 22], corresponding to possible entanglement lengths of 80 and 150 photons. The second work reports also 0.65 collected photons per pump pulse, suggesting the detection of a 32 photon event every second for the 82 MHz pumping rate. In practice, the overall collection and detection efficiencies of these two works are below 1%, limiting the possible detection rate to around 3-4 photon events every second. However, this is in principle a technical limitation that can be improved by better optics and detectors. Overall detection efficiency of about 5% has already been achieved[33, 34], enabling a sixfold event detection every second. Additionally, considering almost perfect detection efficiency[35, 36], a 9 photon event can be detected every second, and 12 every 6 minutes. The short lifetime of single-photon emitters compared to the repetition rate enables photon sources that are pumped by faster lasers[37].

In conclusion, we present a compact time-multiplexed scheme for generating multi-photon linear cluster states, which is realizable with current single-photon sources. It holds promise for better scalability and less need for tunability, and thus the possibility to achieve much larger entangled multi-photon states than it is possible today. A crucial component is a photon-photon entangling gate. Currently, the most efficient gate is obtained by linear optics and post-selection, but there are many efforts pursuing exactly this goal. Finally, we should mention the possibility to append delay loops of different lengths. Such combinations can generate cluster states of higher dimensionality, and even graph states which are useful for the one-way quantum computer scheme. We will describe these options in a future publication.

Gate operation.

Following Fig. 1, a photon is set at the horizontally polarized state $|h\rangle$ at position 1. The photon reaches a CNOT entangling gate, but passes it through with no effect into the delay loop at position 2. When the photon

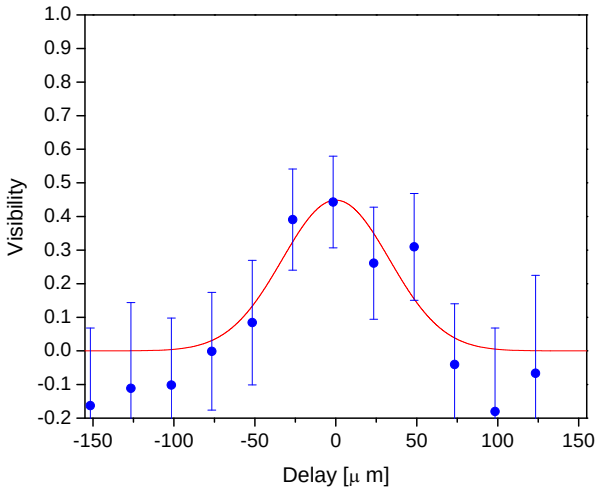

FIG. 5. **Nonlocal interference visibility between three entangled photons.** A constructive (destructive) interference is observed as the delay is scanned, for the $\frac{1}{\sqrt{2}}(|\phi^+h\rangle + |\phi^-v\rangle)$ ($\frac{1}{\sqrt{2}}(|\phi^+h\rangle - |\phi^-v\rangle)$) state. The sixfold signal is composed of the detection of the three heralding photons and the three entangled photons. Each data point was integrated over 34 hours. Event rate was of 1 per 35 minutes at an average pump power of 550 mW. Errors are calculated assuming Poisson distribution.

reaches position 3, it is at the $|p\rangle$ state, after passing a half-wave plate that rotates the polarization by 45°.

Synchronized with the second arrival of this photon to the entangling gate, the single photon source is triggered again such that the two photons are simultaneously entering both input ports of the entangling gate at positions 1 and 3. Photons 1 and 3 are the target and control qubits, respectively. The CNOT gate operation[32] entangles the following states

$$\begin{aligned}
|h_1p_3\rangle &\rightarrow |\phi^+_{24}\rangle = \frac{1}{\sqrt{2}}(|h_2h_4\rangle + |v_2v_4\rangle) \\
|h_1m_3\rangle &\rightarrow |\phi^-_{24}\rangle = \frac{1}{\sqrt{2}}(|h_2h_4\rangle - |v_2v_4\rangle) \\
|v_1p_3\rangle &\rightarrow |\psi^+_{24}\rangle = \frac{1}{\sqrt{2}}(|v_2h_4\rangle + |h_2v_4\rangle) \\
|v_1m_3\rangle &\rightarrow |\psi^-_{24}\rangle = \frac{1}{\sqrt{2}}(|v_2h_4\rangle - |h_2v_4\rangle)\,, \qquad (1)
\end{aligned}$$

thus, the $|h_1p_3\rangle$ state becomes the $|\phi^+_{24}\rangle$ Bell state (indices indicate the photon positions), and entanglement is created between the photon that has left the loop and the other one that is still inside it. After the photon inside the loop is rotated by the wave plate, the source is synchronously triggered for the third time, and the three photon state is $\frac{1}{\sqrt{2}}|h_1\rangle \otimes (|p_3h_5\rangle + |m_3v_5\rangle)$. This time, the entangling operation creates the three photon entangled state $\frac{1}{\sqrt{2}}(|\phi^+_{24}h_5\rangle + |\phi^-_{24}v_5\rangle)$. This is a three photon GHZ state[29], as it can also be written as $\frac{1}{\sqrt{2}}(|h_2h_4p_5\rangle + |v_2v_4m_5\rangle)$.

In order to see the results of adding photons continuously in a similar way, we examine just one more stage. When a fourth photon is added after the photon polarization inside the loop is rotated, the state becomes $\frac{1}{\sqrt{2}}|h_1\rangle \otimes (|p_3h_5p_6\rangle + |m_3v_5m_6\rangle)$. The entangling operation creates a four photon entangled state $\frac{1}{\sqrt{2}}(|\phi^+_{24}h_5p_6\rangle + |\phi^-_{24}v_5m_6\rangle)$, which is actually the linear cluster state $\frac{1}{2}(|h_2h_4h_5p_6\rangle + |v_2v_4h_5p_6\rangle + |h_2h_4v_5m_6\rangle - |v_2v_4v_5m_6\rangle)$. In graph state language, also the two photon Bell state and the three photon GHZ states are linear cluster states. Thus, every additional photon is entangled to the end of the current linear cluster state, extending it by one unit. Interestingly, if the wave-plate in the delay loop is pulled out after the first photon has already passed it, The continuously growing state is of the GHZ type [29]. This pulling out can be achieved be realizing the wave-plate with a Pockels cell.

Experimental PDC setup.

The heralded source generates two photons probabilistically with the PDC process. As we use a PDC source for polarization entangled photons, the generated photons are of horizontal or vertical polarizations randomly. Respectively, we collect data for any sequence combination of input photon polarizations.

The entangling operation in this demonstration is using linear optical elements and post-selection [28]. The optical elements are a PBS with a half-wave plate at 22.5° before one of the input ports. When combined with the post-selection of a single photon coming out of each of the two output ports, this combination entangles both the $|h_1p_3\rangle$ and the $|v_1m_3\rangle$ states into the same $|\phi^+_{24}\rangle$ state, and the $|v_1p_3\rangle$ and the $|h_1m_3\rangle$ states into the $|\phi^-_{24}\rangle$ state.

Maximal indistinguishability, and thus, nonlocal interference, is achieved when the delay time matches the repetition rate of the pump laser. At this length, one photon that has left the delay loop towards the detectors is entangled with the other photon which is still inside the loop. As the first photon which was emitted by the single-photon source was required to pass the PBS into the loop, it was projected onto the $|h\rangle$ state. Thus, this photon's original polarization has no consequences. The polarization of the second emitted photon though, determines whether the final state will be $|\phi^+\rangle$ or $|\phi^-\rangle$. In order to detect these two states, the polarization of both photons should be observed at the $\{|p\rangle, |m\rangle\}$ basis. The first photon that has left the loop is thus rotated by a half-wave plate and detected beyond a second PBS. The polarization state of the other photon which is still in the loop is observed differently. Luckily, the wave plate which is already inside the loop rotates it to the right basis. Its

measurement occurs at the first projecting PBS. If this photon is projected onto the $|h\rangle$ state that corresponds to $|p\rangle$ before the wave plate, it leaves the loop. As there is another wave plate before the second PBS, it will be detected at the next time slot by any one of the two detectors, with equal probabilities. On the other hand, if the second photon is projected onto the $|v\rangle$ state, it will be delayed in the loop for another round, after which it will have equal chances of leaving the loop or staying for another round. Overall, if the second photon is detected in the time slot right after the first one, it was projected onto the $|h\rangle$ state, but if it is detected on any later time, its projection was onto $|v\rangle$.

The three photon interference was observed at the $\{|p\rangle, |m\rangle\}$ basis in a similar way. Additional birefringent phase of 90° was introduced inside the delay loop. See Supplementary Material for further explanations[32].

Acknowledgements The authors would like to thank the Israeli Science Foundation for supporting this work under grants 546/10 and 793/13.

[1] Zhao, Z. et al. Experimental demonstration of five-photon entanglement and open-destination teleportation. *Nature* **430,** 54-58 (2004).

[2] Nielsen, M. A. Optical Quantum Computation Using Cluster States. *Phys. Rev. Lett.* **93,** 040503 (2004).

[3] Yao, X.-C. et al. Observation of eight-photon entanglement. *Nat. Photon.* **6,** 225-228 (2012).

[4] Matthews, J. C. F., Politi, A., Stefanov, A. & OBrien, J. L. Manipulation of multiphoton entanglement in waveguide quantum circuits. *Nat. Photon.* **3,** 346-350 (2009).

[5] Maunz, P. et al. Quantum interference of photon pairs from two remote trapped atomic ions. *Nat. Phys.* **3,** 538-541 (2007).

[6] Lettow, R. et al. Quantum Interference of Tunably Indistinguishable Photons from Remote Organic Molecules. *Phys. Rev. Lett.* **104,** 123605 (2010).

[7] Flagg, E. B. et al. Interference of Single Photons from Two Separate Semiconductor Quantum Dots. *Phys. Rev. Lett.* **104,** 137401 (2010).

[8] Patel, R. B. et al. Two-photon interference of the emission from electrically tunable remote quantum dots. *Nat. Photon.* **4,** 632635 (2010).

[9] Bernien, H. et al. Two-Photon Quantum Interference from Separate Nitrogen Vacancy Centers in Diamond. *Phys. Rev. Lett.* **108,** 043604 (2012).

[10] Portalupi, S. L. et al. Bright Phonon-Tuned Single-Photon Source. *Nano Lett.* **15,** 6290-6294 (2015).

[11] Megidish, E., Shacham, T., Halevy, A., Dovrat, L. & Eisenberg, H. S. Resource Efficient Source of Multiphoton Polarization Entanglement. *Phys. Rev. Lett.* **109,** 080504 (2012).

[12] Walther, P. et al. Experimental one-way quantum computing. *Nature* **434,** 169-176 (2005).

[13] Lounis, B. & Orrit, M. Single-photon sources. *Rep. Prog. Phys.* **68,** 1129 (2005).

[14] Claudon, J. et al. A highly efficient single-photon source based on a quantum dot in a photonic nanowire. *Nat. Photon.* **4,** 174-177 (2010).

[15] Liebermeister, L. et al. Tapered fiber coupling of single photons emitted by a deterministically positioned single nitrogen vacancy center. *Applied Physics Letters* **104,** 031101 (2014).

[16] Sapienza, L., Davanço, M., Badolato, A. & Srinivasan, K. Nanoscale optical positioning of single quantum dots for bright and pure single-photon emission. *Nat. Commun.* **6,** 7833 (2015).

[17] Somaschi, N. et al. Near optimal single photon sources in the solid state. *Nat. Phot.* (2016).

[18] Schreiber, A. et al. A 2D quantum walk simulation of two-particle dynamics. *Science* **336,** 55 (2012).

[19] Rohde, P. P. Simple scheme for universal linear-optics quantum computing with constant experimental complexity using fiber loops. *Phys. Rev. A* **91,** 012306 (2015).

[20] Santori, C., Fattal, D., Vučković, J., Solomon, G. S. & Yamamoto, Y. Indistinguishable photons from a single-photon device. *Nature* **419,** 594-597 (2002).

[21] Gazzano, O. et al. Entangling Quantum-Logic Gate Operated with an Ultrabright Semiconductor Single-Photon Source. *Phys. Rev. Lett.* **110,** 250501 (2013).

[22] Wei, Y.-J. et al. Deterministic and Robust Generation of Single Photons from a Single Quantum Dot with 99.5% Indistinguishability Using Adiabatic Rapid Passage. *Nano Lett.* **14,** 6515-6519 (2014).

[23] Volz, T. et al. Ultrafast all-optical switching by single photons. *Nat. Photon.* **6,** 605-609 (2012).

[24] Englund, D. et al. Ultrafast Photon-Photon Interaction in a Strongly Coupled Quantum Dot-Cavity System. *Phys. Rev. Lett.* **108,** 093604 (2012).

[25] Chen, W. et al. All-Optical Switch and Transistor Gated by One Stored Photon. *Science* **341,** 768-770 (2013).

[26] Baur, S., Tiarks, D., Rempe, G. & Dürr, S. Single-Photon Switch Based on Rydberg Blockade. *Phys. Rev. Lett.* **112,** 073901 (2014).

[27] Shomroni, I. et al. All-optical routing of single photons by a one-atom switch controlled by a single photon. *Science* **345,** 903-906 (2014).

[28] Pan, J.-W., Daniell, M., Gasparoni, S., Weihs, G. & Zeilinger, A. Experimental Demonstration of Four-Photon Entanglement and High-Fidelity Teleportation. *Phys. Rev. Lett.* **86,** 4435-4438 (2001).

[29] Greenberger, D. M., Horne, M. A., Shimony, A. & Zeilinger, A. Bells theorem without inequalities. *American Journal of Physics* **58,** 1131-1143 (1990).

[30] Lindner, N. H. & Rudolph, T. Proposal for Pulsed On-Demand Sources of Photonic Cluster State Strings. *Phys. Rev. Lett.* **103,** 113602 (2009).

[31] Prevedel, R. et al. High-speed linear optics quantum computing using active feed-forward. *Nature* **445,** 65-69 (2007).

[32] Elaborated details appear in the supplementary information.

[33] Strauf, S. et al. High-frequency single-photon source with polarization control. *Nat. Photon.* **1,** 704-708 (2007).

[34] Loredo, J. C. et al. Scalable performance in solid-state single-photon sources. *arXiv*:1601.00654 (2016).

[35] Lita, A. E., Miller, A. J., and Nam, S. W. Counting near-infrared single-photons with 95% efficiency. *Opt. Express* **16,** 3032 (2008).

[36] Pernice, W. H. P. et al. High-speed and high-efficiency travelling wave single-photon detectors embedded in nanophotonic circuits. *Nat. Commun.* **3,** 1325 (2012).

[37] Bartels, A., Heinecke, D. & Diddams, S. A. Passively mode-locked 10 GHz femtosecond Ti:sapphire laser. *Optics Letters* **33,** 1905 (2008).

arXiv:1605.06771v1 [quant-ph] 22 May 2016

SUPPLEMENTARY INFORMATION

I. EFFECTS OF IMPERFECTIONS

In what follows we present a detailed analysis of the performance of our scheme under the effect of the main sources of error. These include errors in the initial polarization state of the incoming photons, imperfection of the polarized beam splitter used within the setup, non-ideal indistinguishability of photons, and the simultaneous emission of two photons (instead of one photon) by the single-photon source. Specifically, we show how any of these errors affects the performance of the scheme dependent on the number of photons and on the severity of the imperfection. Our analysis considers the effect of each error source separately. Nevertheless, this provides us enough insight in order to understand which are the main limiting factors of our scheme and what is the expected efficiency of the implementation of our scheme using state of the art single-photon sources. We use three figures of merits in order to quantify the performance of the scheme. The first figure of merit, which we denote by $\mathcal{C}_{1,N}$, is the concurrence of the final two-qubit state of the first and last qubits, which is obtained after measuring all other qubits along the $\hat{y}$ axis. The second figure of merit, which we denote by $\mathcal{L}$, characteristics the "*entanglement length*" of the obtained $N-$qubit linear cluster state, and is defined as the length of the longest linear cluster state for which $\mathcal{C}_{1,N}$ is still positive. The third figure of merit, which is denoted by $\mathcal{F}$, is the fidelity between the obtained $N-$qubit cluster state and the *ideal* $N-$qubit cluster state. Formally, the three figures of merits are defined by

$$\mathcal{C}_{1,N} = \mathcal{C}\left(\mathrm{Tr}_{2,\ldots,N-1}\left(\frac{\Pi_y \rho \Pi_y}{\mathrm{Tr}\left(\Pi_y \rho\right)}\right)\right), \tag{1}$$

$$\mathcal{L} = \max N \quad \text{s.t.} \quad \mathcal{C}_{1,N} > 0, \tag{2}$$

$$\mathcal{F} = \left\langle \psi_{ideal} \right| \rho \left| \psi_{ideal} \right\rangle, \tag{3}$$

where $\Pi_y = \mathbb{I}_1 \otimes \prod_{i=2}^{N-1} \left|\uparrow_y^i\right\rangle \left\langle\uparrow_y^i\right| \otimes \mathbb{I}_N$, $\mathcal{C}$ is the concurrence, and $\left|\psi_{ideal}\right\rangle$ is the ideal $N-$qubit cluster state.

A. Distinguishability of photons

The desired interference between two post-selected photons can be obtained with certainty only when the two photons are identical in all of their non-polarization degrees of freedom. These include their frequency, spatial and temporal modes. When the photons differ in some of their non-polarization degrees of freedom the probability of interference is decided by the mean magnitude-squared overlap between the wave-functions of the photons, which quantifies the photons' "*probability of indistinguishability*".

Consider a single photon in a pure state, which can be described by

$$\left|\omega_i\right\rangle = \int_{-\infty}^{+\infty} d\upsilon \phi_{\omega_i}\left(\upsilon\right) \left|\upsilon\right\rangle,$$

where $\phi_{\omega_i}\left(\upsilon\right)$ is a normalized spectral amplitude function, such that $\int_{-\infty}^{+\infty} d\upsilon \left|\phi_{\omega_i}\left(\upsilon\right)\right|^2 = 1$. The probability of indistinguishability of two independent such photons is given by their squared overlap, $\mathcal{I}_{i,j} = \left|\langle\omega_i|\omega_j\rangle\right|^2$. Similarly, for photons in a mixed state,

$$\rho_i = \int_{-\infty}^{+\infty} d\omega_i f\left(\omega_i\right) \left|\omega_i\right\rangle \left\langle\omega_i\right|,$$

where $f\left(\omega_i\right)$ is a normalized probability distribution, such that $\int_{-\infty}^{+\infty} d\omega_i f\left(\omega_i\right) = 1$, the probability of indistinguishability can be defined by their mean magnitude-squared overlap [2],

$$\mathcal{I} = \mathrm{Tr}\left(\rho_i \rho_j\right) = \iint_{-\infty}^{+\infty} d\omega_i d\omega_j f\left(\omega_i\right) g\left(\omega_j\right) \left|\langle\omega_i|\omega_j\rangle\right|^2.$$

Indeed, the probability of indistinguishability coincides with the interference visibility of the Hong-Ou-Mandel (HOM) dip. In an HOM experiment, the coincidence probability of two independent photons, ρ_i and ρ_j, is given by

$$P_{cc}\left(\delta\tau\right)=\frac{1}{2}\left(1-\mathcal{I}\left(\delta\tau\right)\right),$$

where $\mathcal{I}\left(\delta\tau\right)=\iiiint_{-\infty}^{+\infty}d\omega_i d\omega_j dv_1 dv_2 f\left(\omega_i\right)g\left(\omega_j\right)\phi_{\omega_i}^{*}\left(v_1\right)\phi_{\omega_j}\left(v_1\right)\phi_{\omega_j}^{*}\left(v_2\right)\phi_{\omega_i}\left(v_2\right)e^{-i\delta\tau\left(v_2-v_1\right)}$ is the probability of indistinguishability of the two photons with a time delay of $\delta\tau$ between the arrival time of the photons at the beam splitter. In terms of the initial states of the photons, the visibility is then given by [3]

$$V=\frac{\max_{\delta\tau}P_{cc}\left(\delta\tau\right)-\min_{\delta\tau}P_{cc}\left(\delta\tau\right)}{\max_{\delta\tau}P_{cc}\left(\delta\tau\right)}=\frac{P_{cc}\left(\infty\right)-P_{cc}\left(0\right)}{P_{cc}\left(\infty\right)}=\mathcal{I}\left(0\right)=\mathcal{I}.$$

Note that as $V=\mathcal{I}=\mathrm{Tr}\left(\rho_i\rho_j\right)=\frac{\mathrm{Tr}\left(\rho_i^2\right)+\mathrm{Tr}\left(\rho_j^2\right)-2\left\|\rho_i-\rho_j\right\|^2}{2}$, where $\left\|\rho\right\|^2=\mathrm{Tr}\left(\rho^{\dagger}\rho\right)$, it is clearly seen that the probability of indistinguishability depends on both the purity of the states of the photons and their identicality.

In our experimental setup we considered polarization photonic states, which are entangled by the operation of a PBS and post-selection. Following Mandel [4], we will now show that in our setup, as in an HOM experiment, the probability of indistinguishability is related to normalized coincidence probability by

$$\mathcal{I}=1-g_{p,m}^{2}\left(0\right),$$

where $g_{p,m}^{2}\left(\delta\tau\right)$ is obtained from the normalized second-order correlation function by

$$g_{p,m}^{2}\left(\delta\tau\right)=\iint_{-\infty}^{+\infty}dtd\tau\frac{\left\langle E_{p,3}^{-}\left(t\right)E_{m,4}^{-}\left(t+\tau\right)E_{m,4}^{+}\left(t+\tau\right)E_{p,3}^{+}\left(t\right)\right\rangle}{\left\langle E_{p,3}^{-}\left(t\right)E_{p,3}^{+}\left(t\right)\right\rangle\left\langle E_{p,4}^{-}\left(t+\tau\right)E_{p,4}^{+}\left(t+\tau\right)\right\rangle},$$

and $E_{i,j}^{\pm}$ are the field operators corresponding to a photon with a polarization i at the location j. We note that for the $\left|p_1p_2\right\rangle$ input state, the resulting post-selected state of two indistinguishable photons is the maximally entangled state $\left|\phi_{id}^{+}\right\rangle=\frac{1}{\sqrt{2}}\left(\left|h_3h_4\right\rangle+\left|v_3v_4\right\rangle\right)$, and we thus denote its density matrix,

$$\rho_{id}=\frac{1}{2}\begin{pmatrix}1&0&0&1\\0&0&0&0\\0&0&0&0\\1&0&0&1\end{pmatrix},$$

as the indistinguishable density matrix, where the rows correspond to the states $\left|p_3p_4\right\rangle$, $\left|p_3m_4\right\rangle$, $\left|m_3p_4\right\rangle$, and $\left|m_3m_4\right\rangle$. Similarly, the resulting state of two fully distinguishable photons is given by the mixed state

$$\rho_d=\frac{1}{4}\begin{pmatrix}1&0&0&1\\0&1&1&0\\0&1&1&0\\1&0&0&1\end{pmatrix}.$$

A general resulting state,

$$\rho=\begin{pmatrix}\rho_{11}&0&0&\rho_{14}\\0&\rho_{22}&\rho_{23}&0\\0&\rho_{32}&\rho_{33}&0\\\rho_{41}&0&0&\rho_{44}\end{pmatrix},$$

can therefore be decomposed as

$$\rho=p_{id}\rho_{id}+p_d\rho_d,$$

where $p_{id} = \mathcal{I}$ is the probability of indistinguishability, and $p_{id} + p_d = 1$. From this we conclude that

$$p_{id} = \rho_{11} + \rho_{44} - \rho_{22} - \rho_{33}.$$

The calculation of the normalized coincidence probability yields

$$g^2_{p,m}(0) = \frac{\mathrm{Tr}\left(a^\dagger_{p,3} a^\dagger_{m,4} a_{m,4} a_{p,3} \rho\right)}{\mathrm{Tr}\left(a^\dagger_{p,3} a_{p,3} \rho\right) \mathrm{Tr}\left(a^\dagger_{m,4} a_{m,4} \rho\right)} = 4\rho_{22} = p_d,$$

and hence [**?**],

$$\mathcal{I} = 1 - g^2_{p,m}(0).$$

For example, in the case of a two-level system (TLS) single-photon source it can be shown that $g^2(0) = 1 - \frac{T_2}{2T_1}$, so $\mathcal{I} = \frac{T_2}{2T_1}$ [5]. In the case of heralded single-photons emitted by a SPDC setup, the probability of indistinguishability is given by $\mathcal{I} = \frac{\sigma_{int}}{\sigma}$, where $\sigma = \sqrt{\sigma^2_{int} + \sigma^2_{ext}}$, σ_{int} is the (transform-limited) Gaussian width of the photon's spectrum (intrinsic width), and σ_{ext} is the Gaussian width of the spectrum of the center frequency, resulting by tracing out the state of the detected twin photon (extrinsic width) [2].
In terms of the post-selected state, the visibility (in the $\{p, m\}$ basis) is given by

$$V_{p.s} = \mathrm{Tr}\left(\sigma_z \otimes \sigma_z \rho\right) = \rho_{11} + \rho_{44} - \rho_{22} - \rho_{33} = \mathcal{I}$$

and indeed, by the definition of $V_{p.s} = \frac{P_{same} - P_{opp}}{P_{same} + P_{opp}}$, where P_{same} (P_{opp}) denote the probability that the two photons arrive at the same (different) polarization, we have that $V_{p.s} = P^{max}_{same} - P^{min}_{opp} = 1 - 2P^{min}_{opp} = 1 - (1 - \mathcal{I}(0)) = \mathcal{I}$.
The probability of indistinguishability can also be interpreted by modeling the photon's state (of all of its other degrees of freedom) as a mixd state of uniformly distributed (orthogonal) modes. In this case $\mathcal{I}$ is just the probability that the two photons have the same mode, and hence, the "*number of modes*" is given by

$$N_m = \frac{1}{\mathcal{I}},$$

which also implies the relation

$$g^2_{p,m}(0) = \frac{N_m - 1}{N_m}.$$

In this picture, the post-selected process of the PBS can be described by

$$\varepsilon(\rho) = \frac{1}{N_m} \varepsilon_0 \rho \varepsilon_0 + \frac{N_m - 1}{2N_m} \left(\varepsilon_0 \rho \varepsilon_0 + \varepsilon_1 \rho \varepsilon_1\right),$$

where $\varepsilon_0 = \sigma_0 \otimes \sigma_z + \sigma_z \otimes \sigma_0$ describes the desired process, and $\varepsilon_1 = \sigma_0 \otimes \sigma_0 + \sigma_z \otimes \sigma_z$, which means that the process $\frac{1}{2}\left(\varepsilon_0 \rho \varepsilon_0 + \varepsilon_1 \rho \varepsilon_1\right)$ takes the input polarization state $|p\rangle_1 |p\rangle_2$ to the (equally) *mixed* state of the output states $|h\rangle_3 |h\rangle_4$ and $|v\rangle_3 |v\rangle_4$. In Fig. 1 and Fig. 2 we plot $\mathcal{C}$ and $\mathcal{F}$ as a function of the number of photons for a fixed number of modes, while in Fig. 3 and Fig. 4 we plot $\mathcal{C}$ and $\mathcal{F}$ as a function of the number of modes for a fixed number of photons. $\mathcal{L}$ as function of N_m is shown in Fig. 2 in the main text.

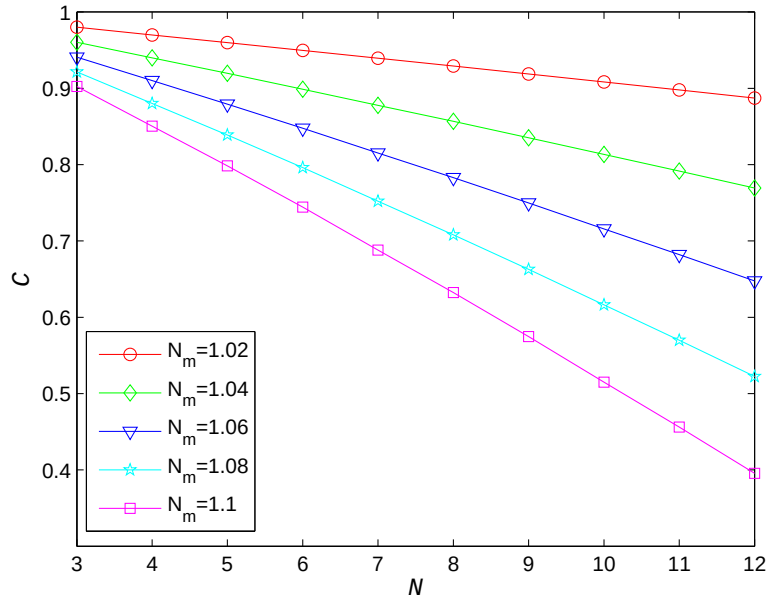

Figure 1. $\mathcal{C}$ as a function of the number of photons.

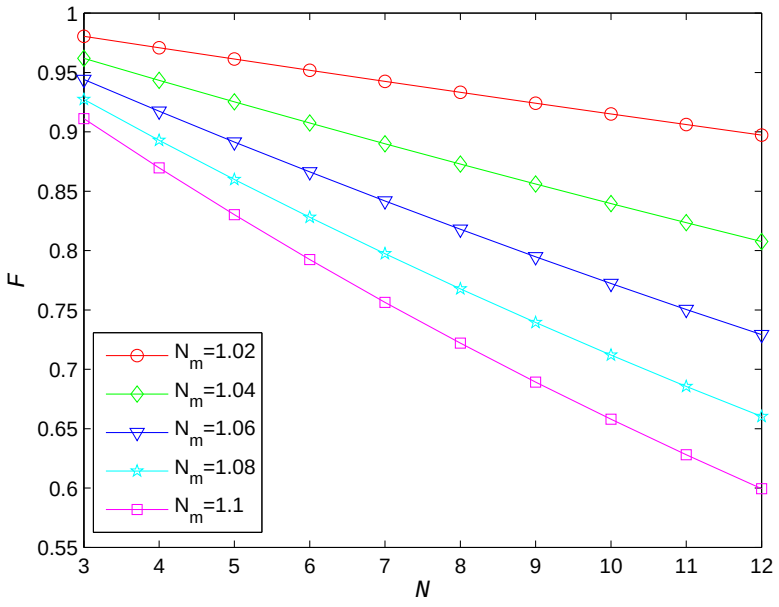

Figure 2. $\mathcal{F}$ as a function of the number of photons.

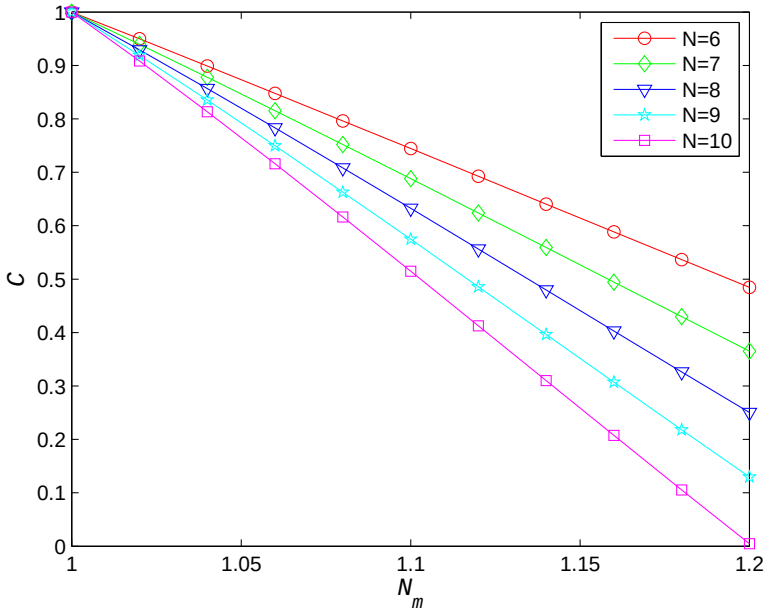

Figure 3. $\mathcal{C}$ as a function of the number of modes.

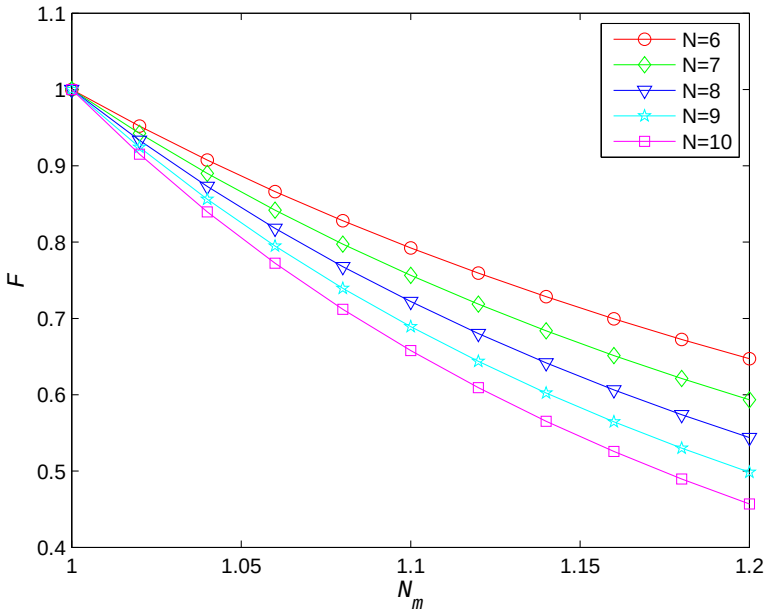

Figure 4. $\mathcal{F}$ as a function of the number of modes.

B. Polarization errors

Ideally, the initial polarization state of each photon which enters the setup is a $|p\rangle = \frac{1}{\sqrt{2}}(|h\rangle + |v\rangle)$ state ($|h\rangle$ ($|v\rangle$) represent horizontal (vertical) polarization and for further use we define $|m\rangle = \frac{1}{\sqrt{2}}(|h\rangle - |v\rangle)\}$). However, errors in the preparation will result in imperfect polarization states. These errors are usually caused by the presence of entanglement between a photon's polarization and its other degrees of freedom, or an entanglement between a photon and its environment (as is the case in photons emitted by parametric down-conversion). We model these polarization errors by a depolarizing quantum channel [1],

$$\varepsilon(\rho) = (1-p)\,\rho + \frac{p}{3}\left(\sigma_x\rho\sigma_x + \sigma_y\rho\sigma_y + \sigma_z\rho\sigma_z\right),$$

ρ is the density matrix, and assume that each photon undergoes a depolarizing channel before it enters the setup. $\mathcal{C}_{1,N}$ and $\mathcal{F}$ as function of the number of qubits for different values of p are shown in Fig. 5 and Fig. 6 respectively. $\mathcal{L}$ as function of p is shown in Fig. 7.

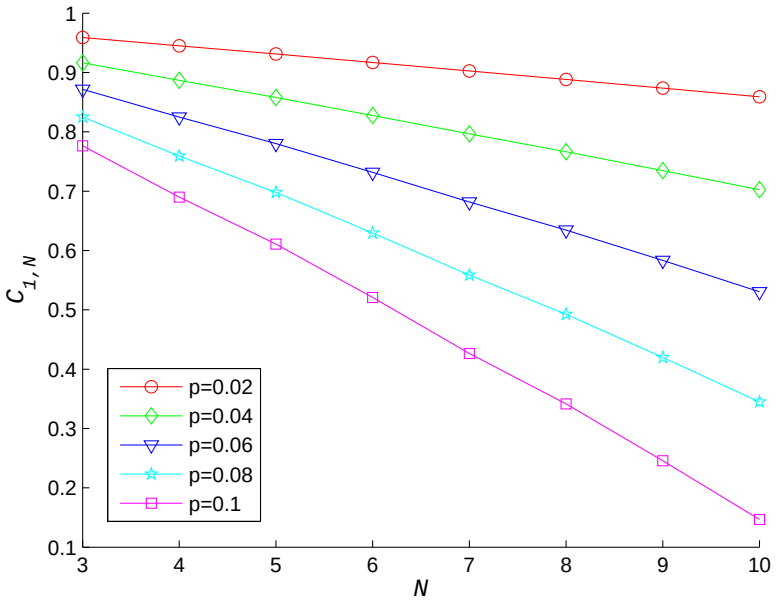

Figure 5. $\mathcal{C}_{1,N}$ as a function of the number of qubits for different values of p (depolarizing channel).

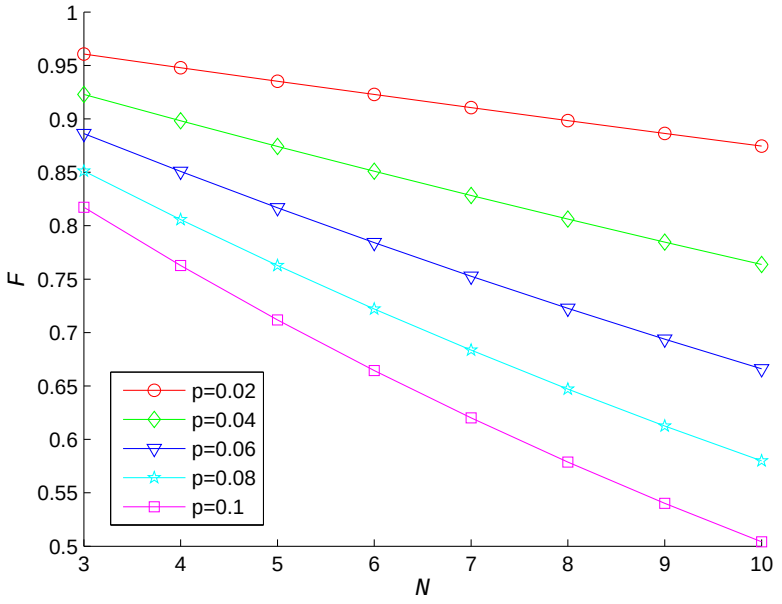

Figure 6. $\mathcal{F}$ as a function of the number of qubits for different values of p (depolarizing channel).

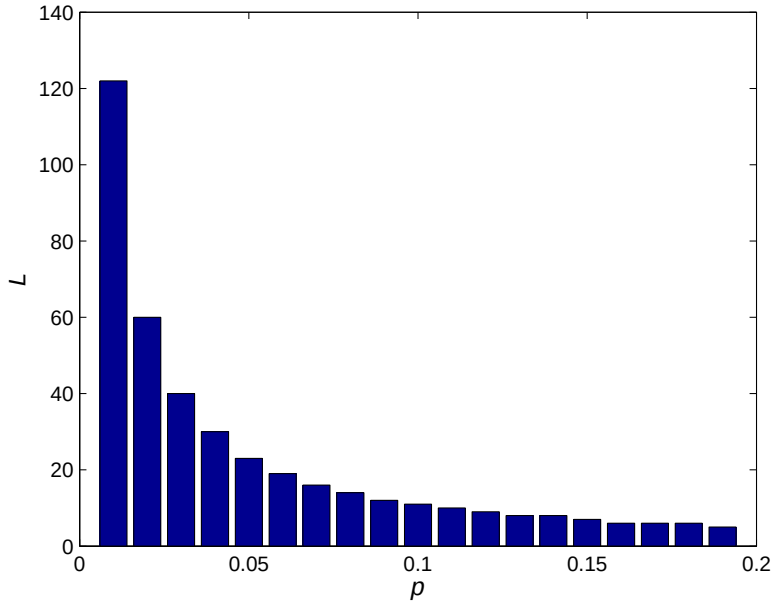

Figure 7. $\mathcal{L}$ as a function of p (depolarizing channel).

Polarization errors can be compensated by adding a polarization filter. Of course, this will result in a better accuracy but with a lower efficiency.

C. Imperfect polarization beam splitter

An ideal PBS transmits only horizontally polarized photons and reflects only vertically polarized photons. In practice, however, horizontally (vertically) polarized photons are also reflected (transmitted). For example, a horizontally polarized photon which enters the PBS from the first input undergoes the transformation

$$|h\rangle_1 \rightarrow t_h |h\rangle_3 + i r_h |h\rangle_4 ,$$

where the indices 1 and 2 (3 and 4) represent the input (output) ports. Similarly, a vertically polarized photon which enters the second input port undergoes the transformation

$$|v\rangle_2 \rightarrow t_v |v\rangle_4 + i r_v |v\rangle_3 ,$$

where for an ideal PBS $t_h = r_v = 1$, and $r_h = t_v = 0$. In our setup we consider the scenario in which one photon enters the PBS from the first input port and another photon enters the PBS from the second input port. In addition, the post-selection ensures that one photon leaves the PBS from the third port and one photon leaves the PBS from the fourth port. The post-selected operation of the PBS is therefore given by the two-qubit transformation

$$T_{PBS} = \begin{pmatrix} t_h^2 - r_h^2 & 0 & 0 & 0 \\ 0 & t_h t_v & -r_h r_v & 0 \\ 0 & -r_h r_v & t_h t_v & 0 \\ 0 & 0 & 0 & t_v^2 - r_v^2 \end{pmatrix},$$

where the first, second, third and fourth rows correspond to the input states $|h_1 h_2\rangle$, $|h_1 v_2\rangle$,$|v_1 h_2\rangle$, and $|v_1 v_2\rangle$ respectively. For typical PBS $t_h^2 = 0.95$ and $r_v^2 = 0.99$, and for high-performance PBS $t_h^2 = 0.98$ and $r_v^2 = 0.995$. Plugging these values in T_{PBS} we obtain $\mathcal{C}_{1,N}$ and $\mathcal{F}$ as function of the number of qubits (See Fig. 8 and Fig. 9). The entanglement lengths of the typical PBS and high-performance PBS are (due to the unitary operation involved - a negligible amount of entanglement resides, in this calculation it is addressed with a numerical threshold of $\mathcal{C}_{1,N} > 10^{-2}$, which is set according to measurement accuracy) $\mathcal{L} = 75$ and $\mathcal{L} = 185$ respectively. We can therefore conclude that the imperfection of the PBS is not a limiting factor in our scheme.

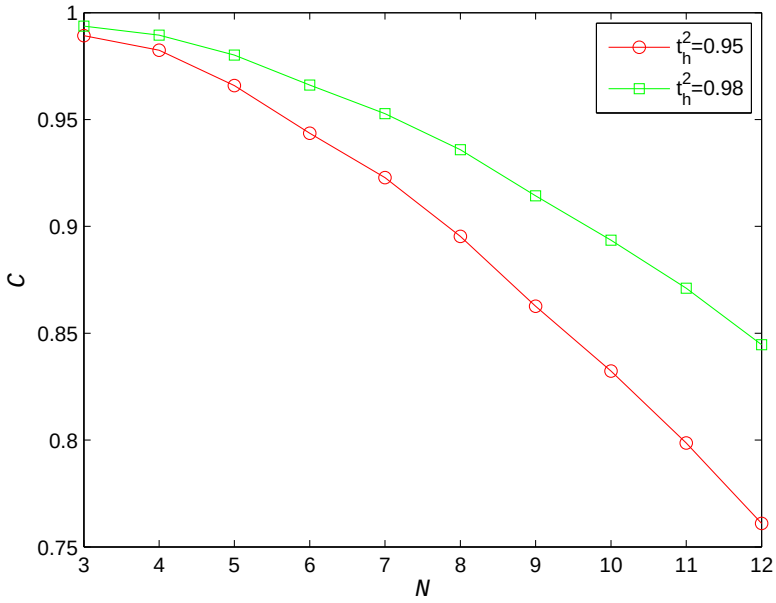

Figure 8. Imperfect PBS - $\mathcal{C}_{1,N}$ as a function of the number of qubits.

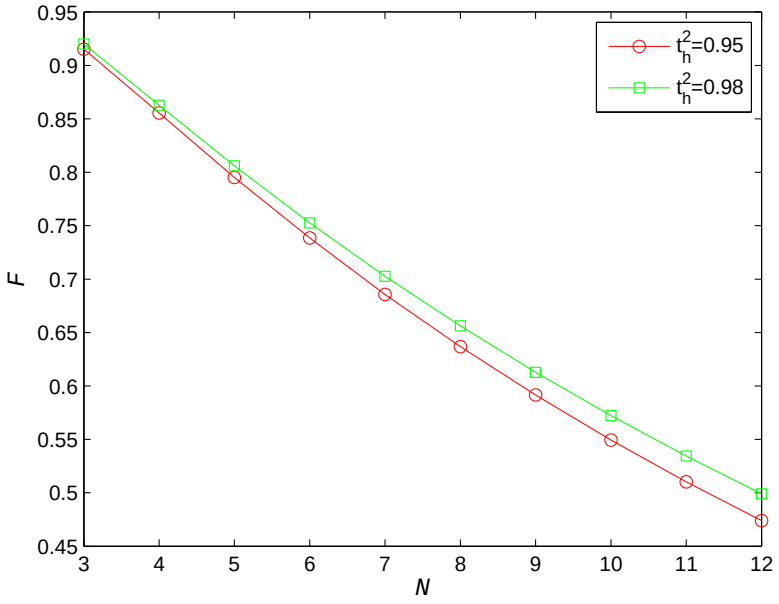

Figure 9. Imperfect PBS -$\mathcal{F}$ as a function of the number of qubits.

D. A two-photon error

In this subsection we consider the case when the single-photon source emits two photons and hence, two photons enter the setup and arrive at the PBS simultaneously. We assume that when two photons arrive at a detector simultaneously one of the photons is lost and the other photon is detected (with an equal probability of each photon to be lost or detected). It is easily verified that when only one photon enters the loop and two photons arrive at the detector, the probability of a successful process is $\mathrm{P}_{sp} = 2/3$ .For simplicity, we deduce a lower bound on the total success probability by assuming that whenever two photons enter the loop (except for the last round [**?**]) the probability of a successful process is zero.

Denote by p the probability that the single-photon source emits two photons. For an N-photon cluster state, the probability that two photons will not be emitted at any round is $(1-p)^N$, and the probability for a two-photon emission in each of the rounds is therefore $\left(1-(1-p)^N\right)/N$ (assuming the occurrence of only one event of two-photon emission during the generation of one cluster-state). Hence, we conclude that the total probability for a successful process is bounded by

$$\mathrm{P}_{sp}^{total} \geq (1-p)^N + \frac{\left(1-(1-p)^N\right)(N-1)}{N}\frac{1}{3} + \frac{\left(1-(1-p)^N\right)}{N}\frac{2}{3}.$$

For commonly used single-photon sources $p \approx 0.01$. In Fig. 10 we plot P_{sp}^{total} as function of the number of qubits.

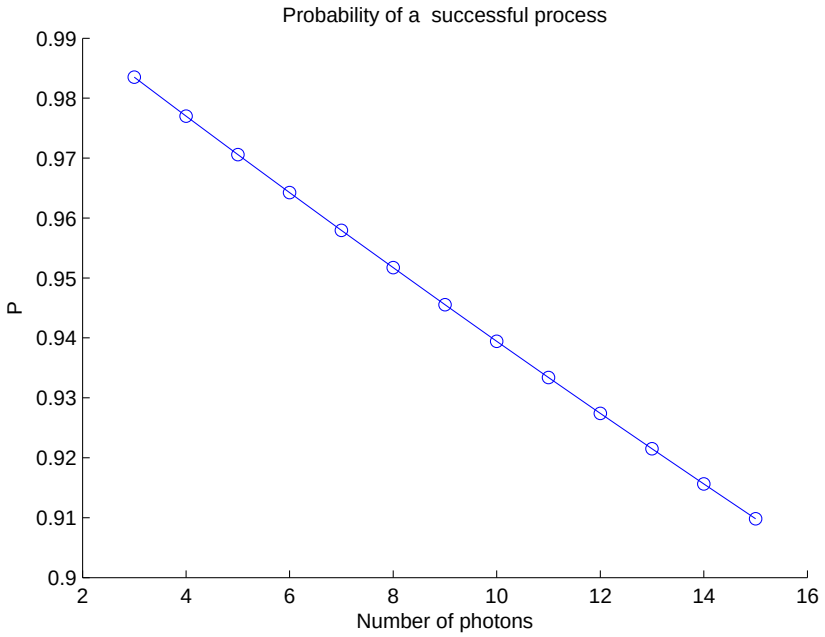

Figure 10. Lower bound on the probability for a successful generation of an N-qubit cluster state given a non-zero probability ($p = 0.01$) for a two-photon emission by the single-photon source.

E. CNOT error

Most generally, our scheme is formulated such that the photons are entangled by a CNOT gate (See Fig. 1 in main text). In this section we consider the effect of an error in the CNOT operation. We model the CNOT operation by

$$U_{CNOT} = \begin{pmatrix} 1 & 0 & 0 & 0 \\ 0 & 1 & 0 & 0 \\ 0 & 0 & \cos\left(\frac{\pi}{2}+\epsilon\right) & i\sin\left(\frac{\pi}{2}+\epsilon\right) \\ 0 & 0 & i\sin\left(\frac{\pi}{2}+\epsilon\right) & \cos\left(\frac{\pi}{2}+\epsilon\right) \end{pmatrix},$$

where ϵ represents the error. An ideal CNOT gate is obtained when $\epsilon = 0$. Averaging over ϵ is obtained by assuming that in each execution of a CNOT gate the density matrix evolves such that with a probability of $1/2$ an ideal CNOT is executed, and with a probability of $1/2$ a faulty CNOT with an error of epsilon is executed (for a given value of ϵ this corresponds to an averaging of the error from zero to epsilon). In Fig. 11 and Fig. 12 we plot $\mathcal{L}$ as a function of ϵ.

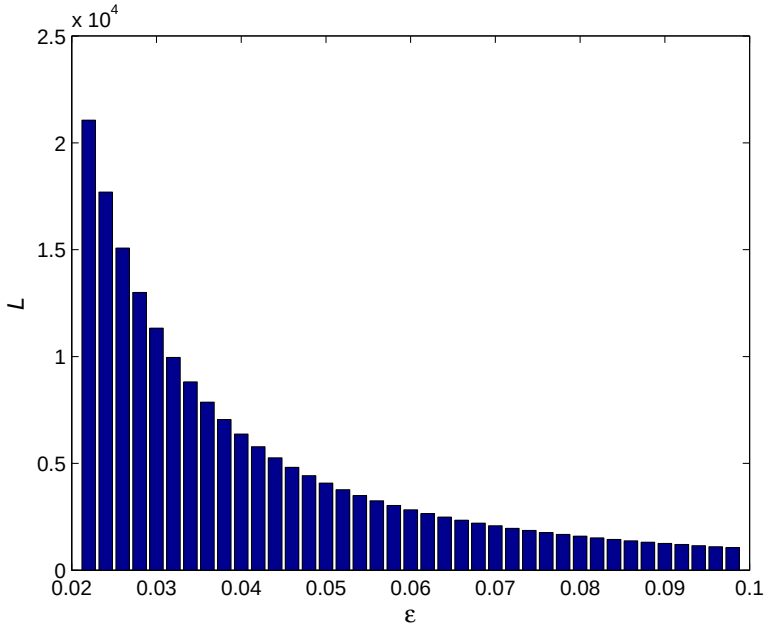

Figure 11. $\mathcal{L}$ as a function of ϵ , $0.022 \leq \epsilon \leq 0.098$.

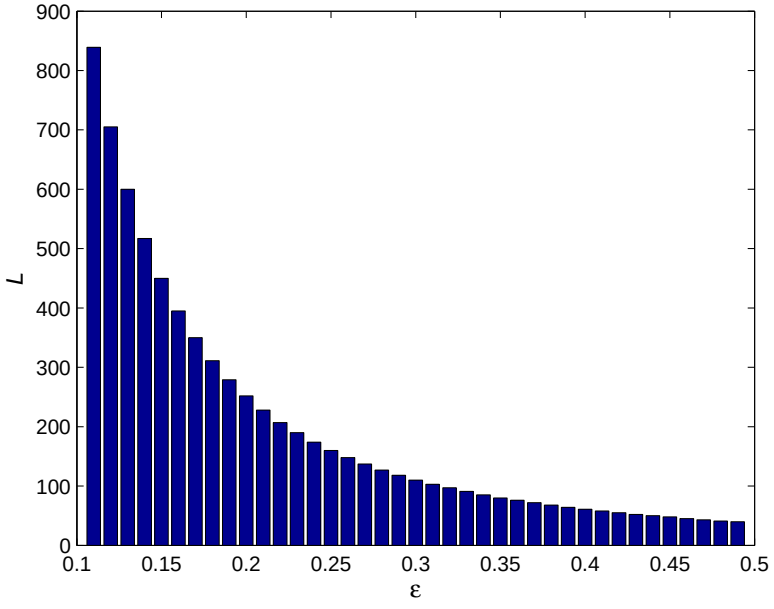

Figure 12. $\mathcal{L}$ as a function of ϵ , $0.11 \leq \epsilon \leq 0.49$.

II. GATE OPERATION

Following the main text and Methods section, the operation performed is described in the following way. We first define the Hadamard transform matrix

$$H = \frac{1}{\sqrt{2}} \begin{pmatrix} 1 & 1 \\ 1 & -1 \end{pmatrix},$$

and the CNOT operation is

$$U_{CNOT} = \begin{pmatrix} 1 & 0 & 0 & 0 \\ 0 & 1 & 0 & 0 \\ 0 & 0 & 0 & 1 \\ 0 & 0 & 1 & 0 \end{pmatrix},$$

The gate operation described in Fig. 1 in the main text is

$$U_{gate} = (H \otimes H)^{-1} U_{CNOT} (H \otimes H)$$

so when the first two photons arrive at paths 1 and 3, for example at the state $|h_1 h_3\rangle$ (the other possibilities could be found in the main text), the resulting state is

$$|\phi\rangle = U_{gate} (I_2 \otimes H) |h_1 h_3\rangle$$

where

$$I_2 = \begin{pmatrix} 1 & 0 \\ 0 & 1 \end{pmatrix}$$

This process could be repeated n number of times and produces an entangled linear cluster state of $n+2$ photons. The resulted $n+2$ ($n > 0$) state is

$$|\phi\rangle_{n+2} = \left(U_{gate} \otimes U_I^{\{n\}}\right) \left((I_2 \otimes H) \otimes U_I^{\{n\}}\right) \left(|h\rangle \otimes |\phi\rangle_{n+1}\right)$$

where U_I is defined in the following manner

$$U_I^{\{k+1\}} = I_2 \otimes U_I^{\{k\}}$$

$U_I^{\{k\}} = 1$ for $k = 0$.

We present, for clarity, the obtainable states from the gate operation up to $n = 3$ (five photon linear cluster state):

$$\begin{aligned}
n = 0 \Rightarrow |\phi\rangle_2 = &\ \frac{1}{\sqrt{2}} (\ |hh\rangle + |vv\rangle) = \left|\phi^+\right\rangle \\
n = 1 \Rightarrow |\phi\rangle_3 = &\ \frac{1}{\sqrt{2}} (\ |hhp\rangle + |vvm\rangle) = |GHZ_3\rangle \\
n = 2 \Rightarrow |\phi\rangle_4 = &\ \frac{1}{\sqrt{4}} (\ |hhhp\rangle + |hhvm\rangle + \\
&\qquad |vvhp\rangle - |vvvm\rangle) \\
n = 3 \Rightarrow |\phi\rangle_5 = &\ \frac{1}{\sqrt{8}} (\ |hhhhp\rangle + |hhhvm\rangle + |hhvhp\rangle - |hhvvm\rangle + \\
&\qquad |vvhhp\rangle + |vvhvm\rangle - |vvvhp\rangle + |vvvvm\rangle)
\end{aligned} \tag{4}$$

III. EXPERIMENTAL INTERFERENCE MEASUREMENT

In order to observe the quantum correlation of the entangled state created, an interference measurement was performed. This was obtained by measuring the visibility in the $\{p, m\}$ basis.
For the case of two photon entanglement,where

$$\left|\phi^{+}\right\rangle = \frac{1}{\sqrt{2}}\left(|hh\rangle + |vv\rangle\right)$$

is created (the appropriate subscripts denoting each photon could be found in the main text), a transformation to the $\{p, m\}$ basis would lead to

$$\left|\phi^{+}\right\rangle = \frac{1}{\sqrt{2}}\left(|pp\rangle + |mm\rangle\right)$$

Detection in our scheme (see Fig. 3 in main text) comes after a projection measurement on the $\{h, v\}$ basis and four measurement coincidence outcomes are possible

$$P_{pp}, P_{pm}, P_{mp}, P_{mm}$$

which are normalized probabilities (the density matrix diagonal terms ρ_{ii}). In the case of $|\phi^{+}\rangle$ the outcome would read

$$P_{pp} = 0.5, P_{pm} = 0, P_{mp} = 0, P_{mm} = 0.5$$

The 2-photon visibility is defined as

$$V_2 = P_{pp} + P_{mm} - (P_{pm} + P_{mp})$$

For the case of three photon entanglement, a similar definition of visibility was required to observe the interference of the state. Yet, when examining the resulted state

$$\frac{1}{\sqrt{2}}(|\phi^{+}h\rangle + |\phi^{-}v\rangle) = \frac{1}{\sqrt{2}}(|hhp\rangle + |vvm\rangle)$$

a similar process of transformation, projection and detection would give 8 probabilities

$$P_{ppp}, P_{ppm}, P_{pmp}, P_{pmm}, P_{mpp}, P_{mpm}, P_{mmp}, P_{mmm}$$

that are all equal, thus the visibility $V_3 = 0$ and would not be able to exhibit the existence of quantum correlations as in the two photon case (this does not occur in linear clusters with higher even number of photons).
Overcoming this problem, without changing the measurement process, is possible by introducing a birefringent phase φ in the delay loop. The created two photon state is

$$\left|\phi^{i+}\right\rangle = \frac{1}{\sqrt{2}}\left(|hh\rangle + e^{i\varphi}\,|vv\rangle\right)$$

following the gate operation on the third photon and an addition of the birefringent phase φ in the delay loop, the three photon state is

$$\frac{1}{\sqrt{2}}(|\phi^{i+}h\rangle + e^{i\varphi}|\phi^{i-}v\rangle) = \frac{1}{\sqrt{4}}(|hhh\rangle + e^{i\varphi}|vvh\rangle + e^{i\varphi}|hhv\rangle - e^{i2\varphi}|vvv\rangle)$$

Examining the measurement outcome probabilities in the $\{p, m\}$ basis gives two different dependencies on φ. For $P_{ppp}, P_{pmm}, P_{mpm}, P_{mmp}$ (odd number of p) the dependence is

$$\frac{1}{32}(6 - 2cos(2\varphi))$$

while for $P_{ppm}, P_{pmp}, P_{mpp}, P_{mmm}$ (even number of p) it is

$$\frac{1}{32}(2 + 2cos(2\varphi))$$

It is clear that for the case of $\varphi = 0^\circ$ the two terms are equal, while for $\varphi = 90^\circ$ the first (second) term interferes constructively (destructively). In this way the three photon visibility is defined as

$$V_3 = P_{ppp} + P_{pmm} + P_{mpm} + P_{mmp} - (P_{ppm} + P_{pmp} + P_{mpp} + P_{mmm})$$

Notice, that for the case of $\varphi = 90^\circ$, the 2-photon visibility $V_2 = 0$.

---

[1] Nielsen, M. A. & Chuang, I. L. *Quantum Computation and Quantum Information*. (Cambridge University Press, 2000).
[2] Sun, F. W. & Wong, C. W. Indistinguishability of independent single photons. *Phys. Rev. A* **79,** 013824 (2009).
[3] Ou, Z. Y., Rhee, J.-K. & Wang, L. J. Photon bunching and multiphoton interference in parametric down-conversion. *Phys. Rev. A* **60,** 593-604 (1999).
[4] Mandel, L. Coherence and indistinguishability. *Optics Letters* **16,** 1882 (1991).
[5] Bylander, J., Robert-Philip, I. & Abram, I. Interference and correlation of two independent photons. *Eur. Phys. J. D* **22,** 295-301 (2003).